

NETWORK-LEVEL MEASURES OF MOBILITY FROM AGGREGATED ORIGIN-DESTINATION DATA

ALISHA FOSTER[†], DAVID A. MEYER[‡], ASIF SHAKEEL[‡]

ABSTRACT. We introduce a framework for defining and interpreting collective mobility measures from spatially and temporally aggregated origin–destination (OD) data. Rather than characterizing individual behavior, these measures describe properties of the mobility system itself: how network organization, spatial structure, and routing constraints shape and channel population movement. In this view, aggregate mobility flows reveal aspects of connectivity, functional organization, and large-scale daily activity patterns encoded in the underlying transport and spatial network.

To support interpretation and provide a controlled reference for the proposed time-elapsd calculations, we first employ an independent, network-driven synthetic data generator in which trajectories arise from prescribed system structure rather than observed data. This controlled setting provides a concrete reference for understanding how the proposed measures reflect network organization and flow constraints.

We then apply the measures to fully anonymized data from the NetMob 2024 Data Challenge, examining their behavior under realistic limitations of spatial and temporal aggregation. While such data constraints restrict dynamical resolution, the resulting metrics still exhibit interpretable large-scale structure and temporal variation at the city scale.

1. INTRODUCTION

Human mobility has become a central object of study across the physical and social sciences, driven by the widespread availability of digitally mediated traces of movement from mobile devices, applications, and networked services. Early work in this area relied largely on individual-level records, such as call detail records (CDRs), GPS traces, and application usage logs, which enable the reconstruction of trajectories and the characterization of personal movement patterns. However, growing concerns over privacy and re-identification risk [1, 2] have increasingly constrained access to such fine-grained data. As a result, much contemporary mobility data is released only in aggregated form, reporting collective OD flows between coarse spatial units over fixed time intervals [3, 4].

In these datasets, the study region is partitioned into a spatial grid and the observation period into a sequence of temporal intervals. For each interval, the data typically consist of population counts within grid cells and aggregated trip counts between origin and destination cells, sometimes accompanied by summary statistics such as mean travel distance or time.

[†]DEPARTMENT OF APPLIED MATHEMATICS, UNIVERSITY OF WASHINGTON, SEATTLE, WA 98195-3925, USA

[‡]DEPARTMENT OF MATHEMATICS, UNIVERSITY OF CALIFORNIA, SAN DIEGO, LA JOLLA, CA 92093-0112, USA

E-mail address: alfost@uw.edu, dmeyer@ucsd.edu, ashakeel@ucsd.edu.

Key words and phrases. collective mobility, aggregated origin–destination data, network-level analysis, Markov models, time-elapsd mobility, effective distance, return-to-origin, urban mobility, privacy-preserving data .

This form of aggregation deliberately suppresses individual identities and temporal continuity, revealing mobility only at the collective level. While such representations are well suited to privacy-preserving analysis, they fundamentally alter the questions that can be asked: individual trajectories are no longer observable objects, and mobility must be understood through the structure and evolution of flows on a network of locations. Even when auxiliary information is available, reconstructing or matching individual mobility traces across large-scale datasets has been shown to be fundamentally limited under aggregation, underscoring the loss of identifiability inherent in privacy-preserving mobility representations [5]. At this level of abstraction, mobility is naturally described as flow on a spatial network, where structure and dynamics are intertwined, rather than as collections of individual trajectories [6]. Viewed in this way, aggregated data provide a system-level description of cities as organized, evolving spatial networks, aligning with broader conceptualizations of urban structure as emergent from flows rather than static land use [7].

A substantial body of work has developed models and measures of mobility from individual trajectory data, including displacement statistics, jump-length distributions, radius of gyration, and related long-term indicators [8–10]. Network constraints imposed by urban street topology have also been shown to strongly influence observed displacement statistics, even when individual movement rules are simple [11]. These measures have proven effective in characterizing regularities of personal movement and their predictability. In contrast, the present work is not concerned with reconstructing or approximating individual behavior. Instead, we ask what can be learned about mobility at a macroscopic level—about network organization, connectivity, and the ability of spatial infrastructure to channel population movement—when individuals are observable only through their aggregated contributions to OD flows. Related efforts have also explored mobility measures derived from enriched or hybrid datasets, such as mobile phone records augmented with geographic information systems, highlighting the sensitivity of mobility metrics to data representation and preprocessing choices [12]. From this perspective, the present work is closer in spirit to diffusion and flow processes on temporal networks than to trajectory-based models of individual mobility, with aggregation inducing an effective Markovian description at the population level.

Our objective is therefore to develop *network-level mobility measures* derived entirely from collective OD data. These measures are inspired in spirit by individual-based metrics but differ fundamentally in interpretation: they characterize properties of the mobility system itself, as revealed by population flows, rather than properties of individual movers. In this sense, individuals act as distributed probes of the underlying spatial and temporal structure, allowing collective movement to reveal how effectively the network supports recurring activities, daily rhythms, and longer-term redistribution.

To support this perspective, we introduce a pseudo Markov-chain formulation in which time-indexed OD matrices define a sequence of stochastic flow operators acting on an indistinguishable population. This construction provides a principled way to reason about time-elapsed flows across multiple aggregation intervals while remaining entirely within the collective description imposed by privacy-preserving data release. Building on this framework, we define several mobility measures that summarize cumulative flow behavior, indirectness of movement, and recurrence at the network level.

The measures are examined using mobility data from the NetMob 2024 Data Challenge [13], provided by Cuebiq.¹ This dataset is part of a broader recent effort to promote open, standardized, and comparative human mobility data products, which have expanded opportunities for population-level analysis while also emphasizing the analytical consequences of spatial and temporal aggregation [14]. The dataset covers Mexico, Indonesia, India, and Colombia, and reports population counts and OD flows at multiple spatial and temporal resolutions. In this study, we focus on 3-hourly GH5 OD data for the year 2019. As is typical of strongly aggregated datasets, the data exhibit temporal coarsening and sparsity effects that limit direct interpretability at short time scales. Rather than treating these limitations as obstacles to trajectory reconstruction, we use them to motivate mobility indicators that are robust to aggregation and meaningful at the scale at which the data are available.

To aid interpretation and validate the proposed constructions, we additionally employ a separate, network-driven synthetic data generator in which trajectories arise from externally specified structural and temporal biases. These synthetic trajectories are not intended to model observed behavior; instead, they provide controlled settings in which the relationship between network structure, prescribed dynamics, and resulting mobility measures can be examined explicitly. Related work on collective human mobility from aggregated data has examined flow structures, event-driven patterns, and relationships between short- and long-term movements [15–19]. In contrast, the focus here is not on identifying or classifying behavioral regimes, but on developing time-elapsing measures derived from a pseudo Markov-chain model that remain interpretable under strong spatial and temporal aggregation.

A related study introduces a network-driven Markov mobility generator that produces full synthetic trajectories and validates, in controlled settings, the consistency between trajectory-level realizations and aggregated OD representations [20]. The synthetic datasets used here are generated using the publicly available code from that work; however, the definitions, algorithms, and analyses of time-elapsing mobility measures presented in this paper are self-contained and do not rely on trajectory-level assumptions.

Because the proposed framework is defined entirely at the level of time-dependent Markov transition operators, all time-elapsing mobility measures considered here are fixed by these operators up to finite-sample effects. Comparisons with realized trajectories therefore probe only sampling variability, rather than providing an independent form of empirical validation. Accordingly, validation in this work focuses on internal consistency, identifiability, and reproducibility; all computations are fully specified and supported by publicly available code.

This paper is organized as follows. Section 2 introduces the pseudo Markov-chain framework for spatially and temporally aggregated OD data and discusses limitations arising from temporal aggregation that we define as *mobility-aliasing*. Section 3 develops time-elapsing net flow measures and demonstrates how temporal composition reveals large-scale directional structure in both synthetic and aggregated mobility settings. Section 4 introduces time-elapsing OD distance and the associated notion of effective distance, which serves as a

¹Cuebiq’s terms and conditions for the NetMob 2024 Data Challenge require us to refer the reader to the following statement pertaining to the availability of data: Aggregated data was provided by Cuebiq Social Impact as part of the Netmob 2024 conference. Data is collected with the informed consent of anonymous users who have opted-in to anonymized data collection for research purposes. In order to further preserve the privacy of users, all data has been aggregated by the data provider spatially to the GH3, GH5, h37 and temporally to 3-hourly, daily, weekly, and monthly levels and does not include any individual-level data records.

network-level measure of indirectness and structural inefficiency in collective movement; this section constitutes the primary empirical focus of the paper.

We also describe return-to-origin (RTO) distances as a natural extension of the time-elapsd framework, obtained by specializing OD distances to coincident endpoints. While RTO measures provide a collective analogue of long-term mobility indicators such as radius of gyration, we do not pursue a detailed empirical analysis here, instead outlining their definition and interpretation as a direction for future work.

We conclude in Section 6 with a discussion of implications, limitations, and directions for further research.

2. PSEUDO MARKOV-CHAIN MODEL

To analyze collective mobility using spatially and temporally aggregated OD data, we introduce a pseudo Markov-chain formulation. At the level of aggregation imposed by privacy-preserving data release, individual identities and movement histories are not observable. As a result, mobility can only be described probabilistically in terms of transitions between locations. While the resulting construction resembles a time-inhomogeneous Markov chain, the Markovian structure arises from aggregation and indistinguishability rather than from assumptions about individual behavior [21].

We adopt the term *privacy-enhanced person* (PEP) to denote an abstract realization of this description: a notional, indistinguishable mover whose transitions reflect observed collective flows rather than an identifiable trajectory. PEPs should not be interpreted as approximations to real individuals; instead, they serve as analytical carriers of population flow, providing a convenient representation for reasoning about aggregate mobility without assigning persistent identities.

For each time-step t , we construct a stochastic transition matrix M^t encoding the probability of moving from an origin location to a destination location within that interval. To extend inference beyond single time slices, we define *time-elapsd transition matrices* that capture the cumulative effect of successive flow operators over multiple intervals. These matrices form the basis for estimating longer-term, collective mobility quantities such as net population flow, cumulative travel distance, and recurrence statistics, all defined entirely at the aggregate level.

Depending on the chosen spatial and temporal resolution, observed trips may predominantly occur within metropolitan regions or between distant regions. Consequently, mobility structure is often localized in space and time, and it is natural to focus on connected components at the scales of interest rather than on entire national networks. The pseudo Markov-chain model itself is defined generically for aggregated OD data and is consistent with standard treatments of diffusion and transport on temporal networks, where Markovian structure arises from coarse-graining rather than behavioral assumptions [21, 22].

2.1. Network-Driven Synthetic Data Generator. To support interpretation and validation of the proposed time-elapsd mobility measures, we employ a network-driven synthetic data generator that produces controlled, aggregate OD flows. The goal of this construction is not to reproduce empirical mobility patterns, but to provide a reference setting in which the relationship between network structure, prescribed dynamics, and resulting collective mobility measures can be examined explicitly. For clarity, we first describe a controlled, network-driven synthetic mobility setting that motivates the construction, before introducing empirical aggregated OD data.

The generator is adapted from the network-driven Markov dynamics introduced in [20], where individual mobility trajectories arise from time-dependent stochastic operators defined on a spatial network. In this work, we use the same framework solely to generate aggregated OD flows, without retaining individual identities or paths, and in a form consistent with the privacy-preserving, collective description assumed throughout this paper.

The synthetic mobility network is constructed using the H3 hierarchical hexagonal spatial index [24], rather than the geohash-based grids used in the NetMob dataset. We employ H3 resolution 6 (R6), for which adjacent cell centers are separated by approximately 6.4 km on average, providing a regular and isotropic spatial tessellation suitable for network-based mobility modeling. Time is discretized into 30-minute intervals, a resolution commensurate with typical urban travel speeds at this spatial scale.

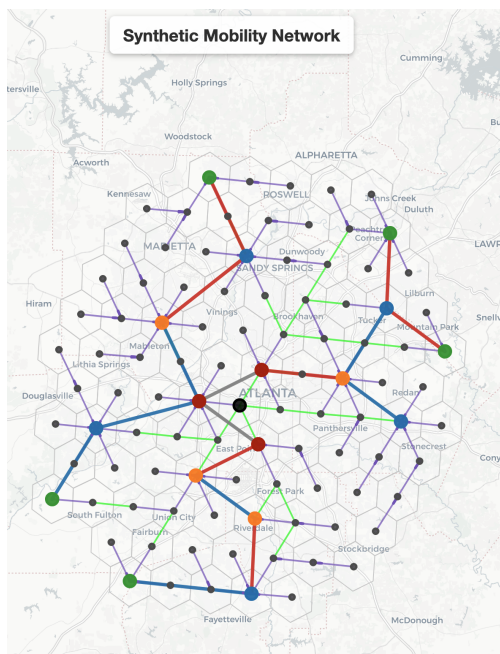


Figure 1. Synthetic mobility network used in all experiments. Nodes correspond to H3 resolution 6 cells over the Atlanta metropolitan area. Thicker nodes denote hub locations, with node color indicating distance bands from the designated center. Thicker edges correspond to high-capacity metro connections, while thinner edges represent local connections. This network serves as the fixed spatial structure on which time-dependent Markov dynamics generate synthetic mobility flows.

Interpretation of synthetic time indices:

For clarity, the calendar dates associated with the synthetic experiments (e.g., 2025-06-01 to 2025-06-29) carry no intrinsic semantic meaning. They are used solely to index a sequence of consecutive time steps and to define a finite range of days over which periodic dynamics are observed. The synthetic data generator does not model real calendar effects, seasonality, or external events, and the choice of dates is arbitrary. All results derived from the synthetic data depend only on the relative ordering and duration of time steps, not on their absolute placement on the calendar.

The network is instantiated over real geographic locations using the Atlanta metropolitan area as a spatial backdrop. Nodes correspond to H3 R6 cells, while edges encode admissible movements defined by a prescribed corridor-and-feeder structure, including hub nodes, high-capacity metro edges between selected hubs, and lower-capacity local connections. Figure 1 shows the resulting network, which is fixed across all synthetic experiments. Full construction details are given in [20].

To induce interpretable large-scale movement patterns, the dynamics incorporate a deliberately simplified center–periphery structure. A small set of cells near a geographic and network-defined reference point is designated as the *center*, while all remaining cells are treated as peripheral. This notion of center is independent of network degree: hub nodes serve a distinct structural role by enabling aggregation and long-range connectivity, and may but need not coincide with central cells.

Mobility is generated by a prescribed, time-varying, gravity-like model defined on a fixed spatial network. At each time-step, locations are assigned activity levels and stay probabilities, and movements are biased toward nearby, higher-activity nodes, with additional structural emphasis placed on hubs and high-capacity corridors. A simple center–periphery potential, defined by graph distance from a selected set of reference cells, provides a consistent notion of inward and outward movement along the network. During morning-like phases, this gravity field preferentially attracts movement toward central locations, while during afternoon and evening phases the bias is partially reversed, favoring outward redistribution. Additional mechanisms—such as elevated stay probabilities at hubs and time-dependent modulation of long-range metro links—promote accumulation, through-flow, and delayed release of population.

The synthetic mobility network is constructed to be strongly connected as a static graph. In addition, the time-dependent mobility dynamics are designed so that the product of transition matrices over one 24-hour cycle is primitive. This guarantees the existence and uniqueness of a periodic fixed point for the time-dependent Markov dynamics [20]. Because the prescribed transition schedule is strictly periodic with a 24-hour cycle, the corresponding time-dependent Markov dynamics admit a periodic fixed point for each of the daily cyclic products starting at any time-step of the day. This fixed point we choose is the one that corresponds to the population distribution at the start of each daily cycle (midnight), expressed as a probability distribution over all spatial tiles in the network. In all synthetic experiments reported here, simulations are initialized at this periodic fixed point, so that observed OD trip-counts for each time-step and ensuing flow calculations reflect the steady cycling behavior of the system rather than transient relaxation. The existence and computation of such periodic fixed points for network-driven Markov mobility models are established in [20].

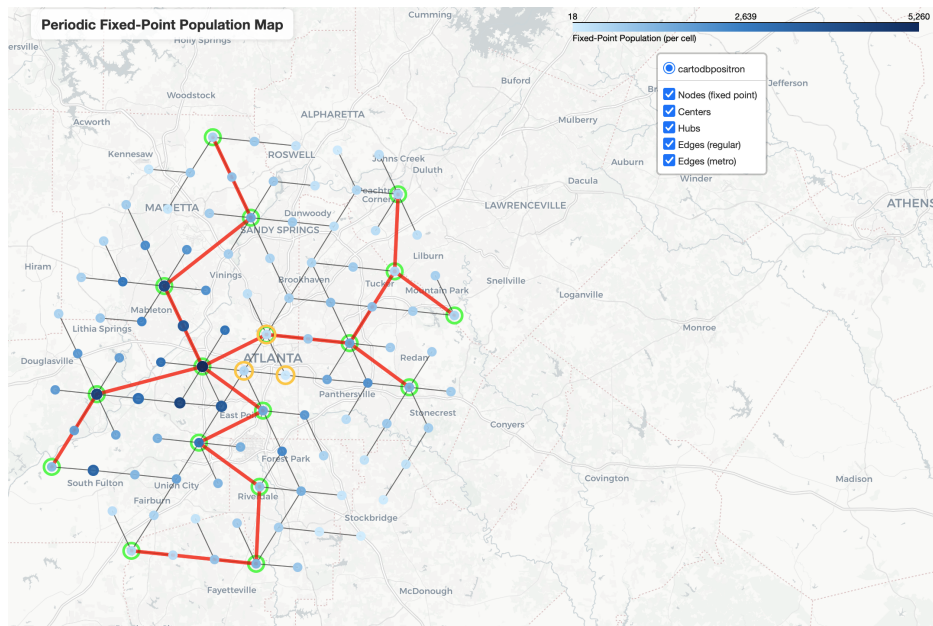


Figure 2. Periodic fixed-point population distribution of the synthetic mobility model, corresponding to the midnight distribution of population-equivalent persons across H3 tiles. Darker colors indicate higher population density. Amber-circled nodes denote the designated center of the network, while all remaining nodes form the periphery.

Synthetic data is realized by simulating 120,000 population-equivalent persons (PEPs) evolving under these dynamics. Resulting trajectories are aggregated into OD matrices at each time-step and over time-elapsing windows. In this paper we work exclusively with the aggregated synthetic OD data; statistical agreement with trajectory-level realizations is established in [20]. All aggregation and visualization procedures are implemented in open-source code.

Because the network structure and temporal biases are prescribed rather than inferred, the resulting OD flows admit direct interpretation. In the sections that follow, we therefore use this synthetic generator to establish reference behavior for time-elapsing net flows, before applying the same constructions to strongly aggregated real-world mobility data.

2.2. Aggregated OD Data. Having introduced the framework and its behavior in a controlled synthetic setting, we now apply the pseudo Markov-chain model to time-indexed, spatially aggregated OD data of the type commonly released in privacy-preserving mobility studies. Such data describe population movement between discrete spatial locations over fixed temporal intervals and arise both from empirical measurement pipelines and from network-driven synthetic mobility generators.

In this paper, we apply the framework to the NetMob 2024 Data Challenge dataset [13, 23], provided by Cuebiq. The dataset reports aggregated OD flows and population counts for several countries, including Mexico, Indonesia, India, and Colombia, at multiple spatial and temporal resolutions. All data are fully anonymized prior to release and contain no individual-level records.

In the NetMob dataset, time is discretized into fixed intervals (3-hourly, daily, weekly, or monthly), and space is discretized into grid cells defined by geohash-based centroids. Spatial

resolutions include GH5 (square grid, side length approximately 4.9 km), GH3 (square grid, side length approximately 156.5 km), and H3 resolution 7 (h37; hexagonal grid, side length approximately 1.41 km). All computations in this paper use the 3-hourly GH5 OD data for the year 2019.

Each trip record is indexed by a triple consisting of a time-step, an origin cell, and a destination cell. For each OD pair, the data include the aggregated trip count as well as summary statistics such as the mean, median, and standard deviation of trip distance and trip duration. OD pairs with trip counts below a threshold of 10 are omitted. As a result, the data do not guarantee that trips observed within the same or consecutive time-steps correspond to distinct individuals. In particular, the same individual may contribute to multiple OD pairs within a single interval or across successive intervals.

For each time-step, the OD data can be represented as a weighted directed graph, with nodes corresponding to locations and edge weights given by trip counts. To extend inference beyond individual time slices and to define meaningful longer-term mobility measures, we organize these graphs into a pseudo Markov-chain structure.

For clarity, in all subsequent comparisons we use the term *aggregated data* to refer specifically to the NetMob 2024 OD data provided by Cuebiq, in contrast to the *synthetic data* generated by the network-driven model described in Section 2.1.

2.3. Model Construction. We now formalize the pseudo Markov-chain construction for generic, time-indexed OD flow data. The formulation is independent of how the OD matrices are obtained and applies equally to empirically measured or synthetically generated aggregate flows.

Consider a sequence of OD flow matrices indexed by discrete time-steps $t = 1, \dots, T$. Let N denote the total number of spatial locations. At each time-step t , the OD data define a weighted directed graph on these locations, with edge weights representing aggregated flow counts.

Let f_{ij}^t denote the observed flow from origin location j to destination location i during time-step t . For each origin j , we define a time-dependent transition probability to destination i by normalizing the outgoing flows,

$$m_{ij}^t = \frac{f_{ij}^t}{\sum_{i=1}^N f_{ij}^t}, \quad (1)$$

whenever the denominator is nonzero. The resulting matrix

$$M^t = [m_{ij}^t] \quad (2)$$

is column-stochastic and represents a one-step transition operator acting on an indistinguishable population at time-step t .

Mobility flows often concentrate within subsets of locations over the time scales of interest. We therefore restrict attention to strongly connected components of the directed graph obtained by aggregating edges over multiple time-steps. Let E^t denote the set of directed edges observed at time-step t , and define

$$E_T = \bigcup_{t=1}^T E^t.$$

Let C be a strongly connected component of the graph defined by E_T , with $N_C = |C|$ nodes. All subsequent constructions are performed on C , ensuring that the resulting transition operators are irreducible and free of absorbing states.

Assuming conditional independence of PEP transitions across time-steps given the time-dependent transition operators inferred from aggregated flows, the time-elapsed transition matrix up to time-step t is defined by

$$A^t = \prod_{k=1}^t M^k = M^t A^{t-1}, \quad A^0 = \mathbb{I}. \quad (3)$$

The matrix A^t encodes cumulative transition probabilities over successive intervals and provides the foundation for time-elapsed, flow-based mobility measures.

2.3.1. Aggregation-Induced Limitations and Mobility-Aliasing. A key limitation of strongly aggregated OD data arises from the mismatch between the temporal resolution of the data and the typical speeds of movement. At a given aggregation interval, individuals may traverse multiple spatial cells, while the OD data record only coarse OD transitions.

This effect is evident in the NetMob 3-hourly GH5 data. Median travel distances and durations imply typical travel times between adjacent cells that are substantially shorter than the aggregation interval, allowing an individual to contribute to multiple OD pairs within a single time-step or across successive time-steps. As a result, the same individual may be repeatedly counted as part of distinct aggregated trips.

We refer to this phenomenon as *mobility-aliasing*, by analogy with temporal aliasing in signal analysis. Mobility-aliasing is not specific to the NetMob dataset, but is a general feature of strongly aggregated, privacy-preserving mobility data. Reducing it would require finer temporal aggregation or post-processing techniques to infer sub-interval transitions. We outline a possible algorithmic compensation strategy in Appendix B. In the present work, we proceed using the original aggregated data. While this limits interpretability at very short time scales, it remains sufficient for illustrating the pseudo Markov-chain framework and for defining collective, time-elapsed mobility measures at the level of aggregation imposed by privacy-preserving data release.

3. TIME-ELAPSED OD NET FLOWS

In this section, we build on the pseudo Markov-chain model to compute *time-elapsed net flows* between locations. Starting from the total outgoing population at each origin at the beginning of a time-elapsed interval, we estimate the *net* number of trips between each OD pair over that interval. The resulting quantities summarize directional imbalances in collective movement and provide a natural, flow-based description of large-scale mobility structure (readers primarily interested in interpretation may skip the derivation and proceed directly to the figures and discussion in Sections 3.2 and 3.3).

3.1. Derivation. For each ordered OD pair (i, j) , we define the antisymmetric movement function over edges (k, l) in a strongly connected component C at time-step t by

$$s_{kl}^t(i, j) = \delta_i(k)\delta_j(l) - \delta_i(l)\delta_j(k),$$

where δ denotes the Kronecker delta. This function takes value $+1$ at (i, j) , -1 at (j, i) , and zero elsewhere.

Let the set of ordered edges be

$$E^o = \{(i, j) \mid i < j, i, j \in C\}.$$

The probability that a generic individual is at location j at the beginning of the first time-step is estimated as

$$p_j^1 = \frac{\sum_i f_{ij}^1}{\sum_{i,j} f_{ij}^1}, \quad (4)$$

and the probability that this individual transitions from j to i over the time-elapsd interval up to time-step t is

$$p_{ij}^t = p_j^1 a_{ij}^t,$$

where $A^t = [a_{ij}^t]$ is the time-elapsd transition matrix defined in Eq. (3).

Let

$$n^1 = \sum_{i,j} f_{ij}^1 \quad \text{and} \quad n_j^1 = \sum_i f_{ij}^1 = n^1 p_j^1$$

denote the total population and the population at location j at the beginning of the interval, respectively. The mean time-elapsd *net trip-count* over the ordered edges E^o is then given by

$$\begin{aligned} \bar{s}^t(i, j) &= \sum_{k,l} s_{kl}^t(i, j) n^1 p_{kl}^t \\ &= n^1 (p_{ij}^t - p_{ji}^t) \\ &= a_{ij}^t n_j^1 - a_{ji}^t n_i^1. \end{aligned}$$

Positive values of $\bar{s}^t(i, j)$ indicate a net flow from j to i , while negative values indicate net flow in the opposite direction.

3.2. Synthetic validation and interpretation. We first evaluate time-elapsd net flows using the network-driven synthetic mobility generator introduced in Section 2.1. In this controlled setting, both the spatial network and the time-dependent transition biases are specified explicitly, allowing the resulting flow patterns to be interpreted directly in terms of known structural and dynamical features.

Figures 3a and 3b compare morning net flows computed over a single 30-minute interval (06:00–06:30) and a longer time-elapsd window (06:00–12:00), showing the top 75th percentile of net flows. At the single-interval scale, net flows are sparse and localized, with only a small number of edges exhibiting strong directional imbalance. These flows tend to connect nearby locations and do not yet reveal a clear network-level organization.

When the time-elapsd window is extended, a markedly different structure emerges. Dominant net flows organize into a coherent radial pattern directed from peripheral locations toward a small number of central hub nodes. Longer-range edges enter the top 75th percentile, reflecting sustained inflow toward the urban core across successive intervals. This extension sharpens directional structure rather than merely increasing density, as short-range fluctuations are suppressed through temporal composition.

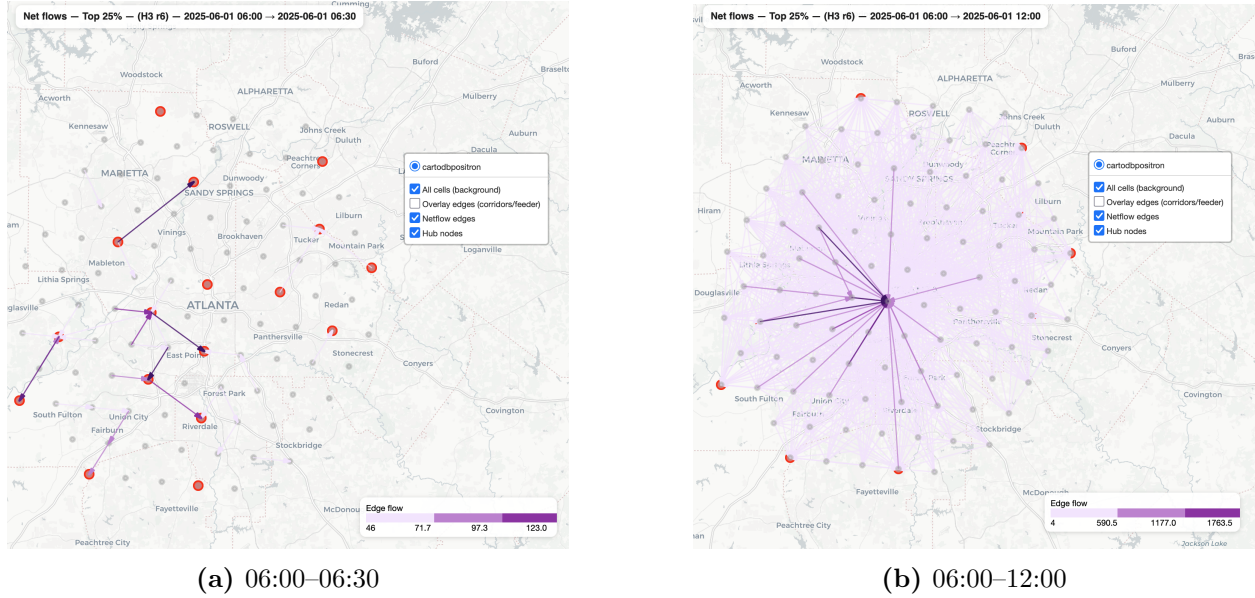


Figure 3. Synthetic morning net flows on an H3 resolution 6 spatial grid. Top 75th percentile of net flows shown. Extending the time-elapsed window transforms sparse, local flows into a coherent radial pattern directed toward central hub nodes, revealing network-scale inbound structure.

Figures 4a and 4b show the corresponding afternoon and evening net flows for the intervals 17:00–17:30 and 17:00–23:00. In the single-interval map, net flows are again weak and fragmented, with no dominant global direction. Edges connect nearby locations, and outward movement from central hubs is only partially visible.

Over the extended time-elapsed window, this pattern reorganizes into a clear outward redistribution from central hub nodes toward the periphery. Compared to the morning period, the flow field is more diffuse, with multiple outgoing directions and a broader spatial spread. Nonetheless, the dominant reversal relative to the morning inflow is clearly resolved, with hub nodes acting as net sources rather than sinks.

This contrast between morning and afternoon phases is particularly sharp in the synthetic setting, reflecting the finer temporal resolution and the absence of long-distance hops within individual time-steps.

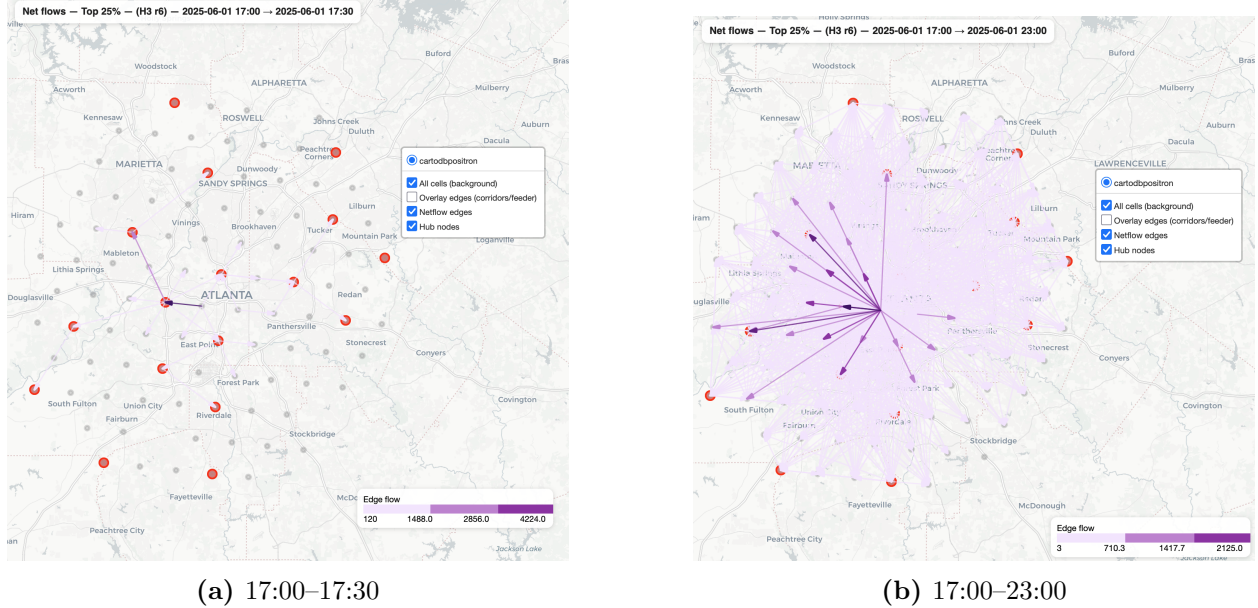


Figure 4. Synthetic afternoon and evening net flows on an H3 resolution 6 grid. Top 75th percentile of net flows shown. Extending the time-elapsed window reveals a clear reversal of dominant flow directions, with outward redistribution from central hubs toward peripheral locations.

Overall, the synthetic results show that, when temporal resolution is commensurate with spatial scale and transitions occur primarily between adjacent locations, time-elapsed net flows can transform weak, local imbalances into coherent, network-scale movement patterns through temporal composition. In this setting, extending the time window sharpens directional organization by suppressing short-term fluctuations arising from stochastic path exploration and reinforcing persistent structural biases encoded in the transition dynamics. These controlled results establish reference behavior for interpreting how time-elapsed net flows behave under less favorable conditions in aggregated mobility data.

3.3. Results from aggregated data. Unlike the synthetic setting, the NetMob data are reported at a coarse temporal resolution of 3 hours, which permits long-distance transitions within a single time-step and weakens the correspondence between temporal aggregation and spatial scale. As a result, short-time dynamics are less directly interpretable, and the behavior of time-elapsed net flows must be assessed under conditions where individual transitions may already span large portions of the metropolitan area.

Figures 5b and 5a compare morning net flows computed over a single 3-hour interval (06:00–09:00) and a longer time-elapsed window (06:00–12:00), showing the top 75th percentile of net flows. In both cases, the dominant net flows are directed toward a small number of central locations, producing dense, radially inward patterns centered on the urban core. When the time-elapsed window is extended from 06:00–09:00 to 06:00–12:00, the set of contributing origins expands outward, with longer-distance flows from the metropolitan periphery entering the top 75th percentile. This shift reflects sustained occupancy of central locations combined with continued inflow from progressively more distant origins, consistent with commuters remaining in the city center while additional arrivals accumulate over time.

By contrast, in the single-interval map, the strongest net flows originate predominantly from locations closer to the center.

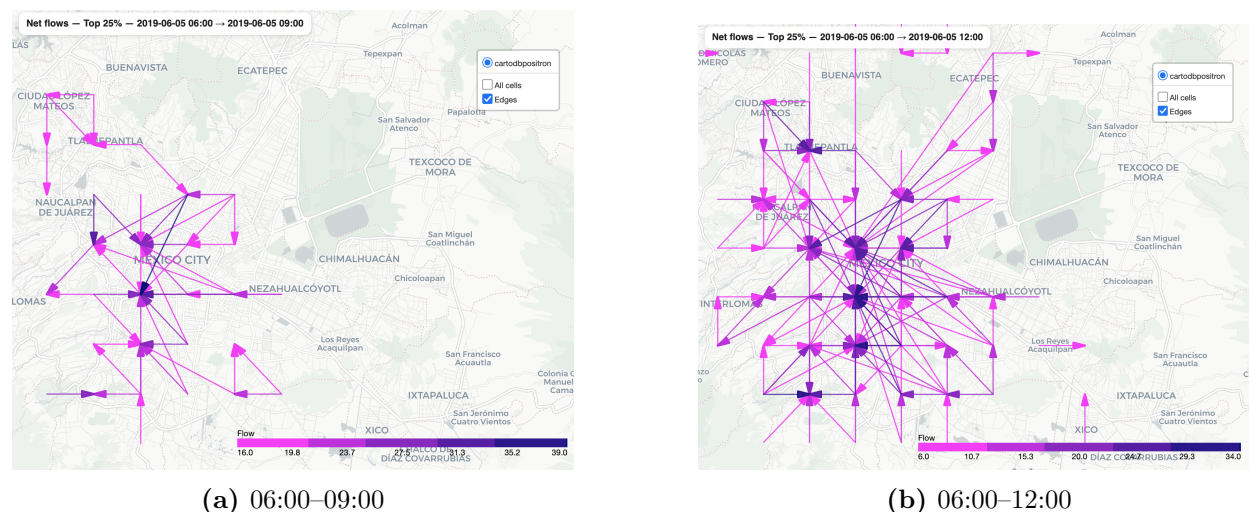


Figure 5. Mexico City, 06–05–2019. Morning time-elapsed net flows showing the top 75th percentile of net flows. Extending the time-elapsed window incorporates longer-distance inflows toward central locations, increasing both the density and spatial reach of inward flows.

Figures 6a and 6b show the corresponding afternoon and evening net flows for the intervals 15:00–18:00 and 15:00–21:00. Relative to the morning period, the dominant flow directions partially reverse: many central locations act as net sources rather than sinks, and outward-directed flows toward peripheral areas become more prominent. This outward redistribution becomes more pronounced as the time-elapsed window is extended, with additional peripheral destinations entering the top 75th percentile.

However, the afternoon and evening patterns are notably less spatially coherent than the morning inflow. Flows are more dispersed in direction, and the radial structure is weaker, reflecting a mixture of return commuting, localized circulation, and residual central activity.

Interpretation.

In contrast to the synthetic case, the aggregated data do not exhibit a stable ordering or recurrence structure across days. The synthetic dynamics show limited stochastic variability due to trajectory sampling; both the set of high effective-distance pairs and their effective-distance magnitudes remain far more stable than in the aggregated setting. We note that this difference is partly a consequence of the deliberately imposed daily periodicity in the synthetic generator. The same framework could be modified to enforce longer periodic cycles (e.g., weekly), which would be expected to produce more heterogeneous recurrence structure more comparable to aggregated data.

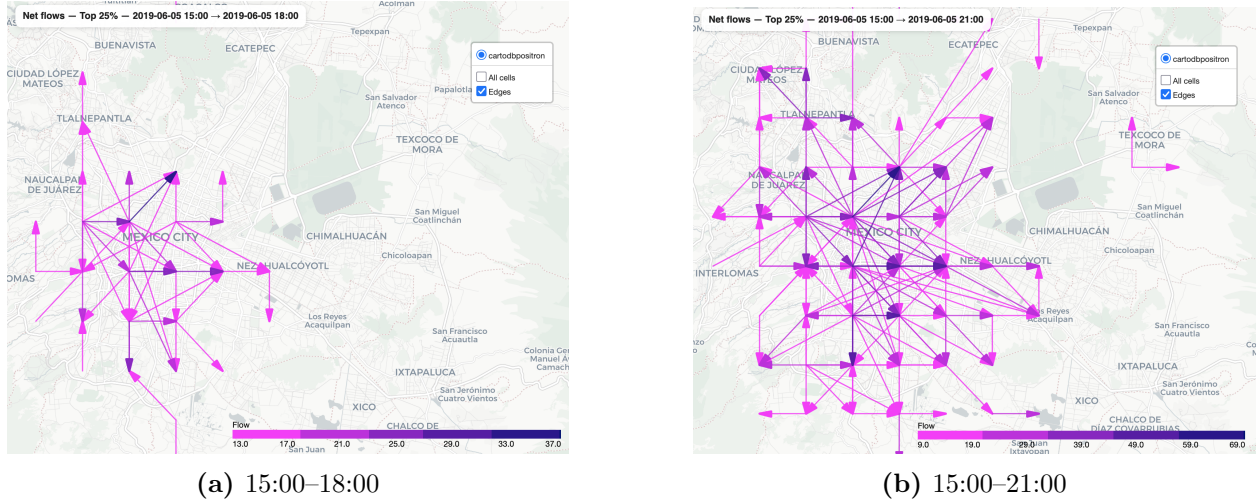


Figure 6. Mexico City, 06–05–2019. Afternoon and evening time-elased net flows showing the top 75th percentile of net flows. Net flow directions partially reverse relative to the morning period, with increased outward redistribution from central locations, though with reduced directional coherence.

Overall, these results illustrate both the utility and the limitations of time-elased net flows when applied to strongly aggregated OD data. While coarse temporal resolution obscures fine-grained movement structure, time-elased net flows nonetheless provide a compact, directional summary of collective redistribution over extended periods, enabling qualitative comparison across time windows and between synthetic and empirical settings.

4. TIME-ELASED OD DISTANCE TRAVELED AND EFFECTIVE DISTANCE

We now extend the time-elased framework beyond trip counts and consider *how far* a PEP travels between an OD pair over a time-elased window. Unlike single-interval distances, which record only direct transitions, time-elased distances incorporate all admissible intermediate paths connecting an origin to a destination, weighted by their probabilities under the underlying mobility dynamics.

This construction captures situations in which travel between two locations systematically deviates from the most direct route, for example due to detours, transfers, congestion, or structural constraints imposed by the mobility network. To compare such effects across OD pairs with widely different geographic separations, we introduce an OD-specific normalization, which we refer to as the *effective distance*.

Throughout this section we focus on travel distance; an identical construction applies to travel time.

4.1. *Time-elased OD distance.* Fix an OD pair (j, i) . We consider all admissible paths that originate at j at the beginning of a time-elased window and first reach i at a later time-step, without passing through either j or i at intermediate times (see Appendix A for the formal recursion).

Let x_{ij}^t denote the mean distance traveled by paths that first reach destination i exactly at time-step t , and let π_{ij}^t denote the probability of such paths. Both quantities are computed

recursively from the single-step transition matrices together with the observed single-step trip distances; the full recursive construction is provided in Appendix A.

The mean distance traveled from j to i over a window $t_1 \leq t \leq t_2$ is defined as the probability-weighted average

$$\bar{x}_{ij}^{t_1, t_2} = \frac{\sum_{t=t_1}^{t_2} x_{ij}^t \pi_{ij}^t}{\sum_{t=t_1}^{t_2} \pi_{ij}^t}. \tag{5}$$

where the denominator is the total probability mass associated with all admissible return paths over the time-elapsd window. For an OD pair (i, j) , this quantity is given by

$$P_{ij}^{t_1, t_2} = \sum_{t=t_1}^{t_2} \pi_{ij}^t,$$

where π_{ij}^t is the probability that a path first reaches i from j at time-step t .

The above expression for $\bar{x}_{ij}^{t_1, t_2}$ represents the expected path length between j and i induced by the mobility dynamics over the time-elapsd window. When the window spans a single time-step, it reduces to the usual mean single-interval trip distance.

We will refer to $P_{ij}^{t_1, t_2}$ as the *total path-hit probability* of the OD pair over the window, and use it as a diagnostic measure of how strongly a given effective-distance connection is supported by the underlying dynamics.

4.2. Normalization and effective distance. Raw time-elapsd distances are not directly comparable across OD pairs, since geographic separation varies substantially. We therefore normalize each time-elapsd distance by an OD-specific baseline, defining the *effective distance*. The term *effective distance* is used here in a descriptive, OD-specific sense and should not be confused with the effective distance introduced in epidemic spreading on networks [25]. While both constructions normalize path length by network structure, the present definition is based on time-elapsd mobility paths inferred from aggregated OD flows rather than on arrival-time geometry of contagion.

A natural baseline is the typical trip distance for the OD pair. However, not all OD pairs realized through time-elapsd paths appear in the single-step data. We therefore impute baseline distances using a regression between geographic distance and observed median trip distance.

Specifically, we perform a weighted linear regression (weighted by trip counts; dominating weight is for self-loops) between geographic distance and median observed trip distance for all OD pairs present in the data. The fitted relation is used to estimate a baseline distance for OD pairs absent from the data. To remain conservative, normalization is performed using the baseline distance plus one standard deviation (or the regression RMSE when imputed).

The effective distance for OD pair (i, j) over window (t_1, t_2) is defined as

$$D_{ij}^{\text{eff}} = \frac{\bar{x}_{ij}^{t_1, t_2}}{\text{baseline}_{ij} + \sigma_{ij}}.$$

Values of effective distance substantially larger than one indicate travel that is systematically longer than expected given geographic separation, signaling indirect, constrained, or inefficient movement between the OD pair.

4.3. *Aggregated data baseline construction.* We apply the effective-distance construction to aggregated OD data from the NetMob 2024 Data Challenge, focusing on the Mexico City metropolitan region and weekday morning commuting windows (06:00–09:00–12:00) throughout 2019.

Figure 7 shows the weighted regression between geographic distance and observed median trip distance. While the fit exhibits substantial variance, it captures the overall trend and provides a workable normalization baseline for effective distance.

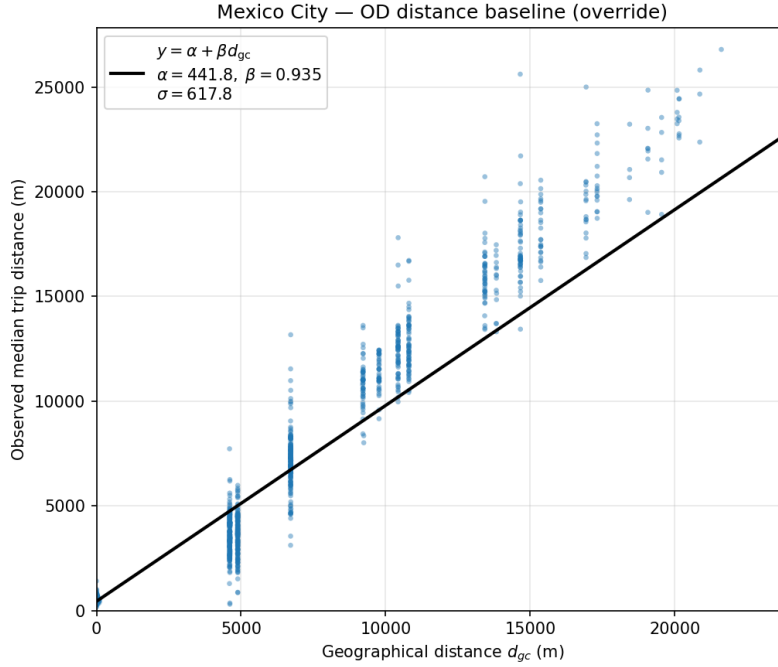


Figure 7. Mexico City: weighted linear fit of observed median trip distance versus geographic distance, used to construct OD-specific effective-distance baselines.

All spatial results and path decompositions are discussed in Section 4.4. Supplementary diagnostics, including temporal persistence of high effective distance OD pairs, are provided in Appendix C.

4.4. *Results: effective distance and path structure.* We now examine time-elapsd effective distances in both synthetic and aggregated settings, focusing on *globally-unconnected pairs* (GUPs), defined as OD pairs that are not connected by a direct single-step transition. Such pairs provide a stringent test of whether effective distance captures structurally indirect travel, rather than merely reflecting geographic separation or the presence of a known direct route.

Synthetic data:

We illustrate the interpretation of effective distance using a synthetic example from the Atlanta network. We consider the time window 06:00–08:00 on 2025–06–01, corresponding to four 30-minute time steps.

Figure 8 shows effective distances for GUPs in the top 99th percentile for that window. The largest value observed is $D_{\max}^{\text{eff}} = 5.36$. Although the corresponding origin and destination

are geographically close, their effective distance is large, indicating a strong topological separation in the network.

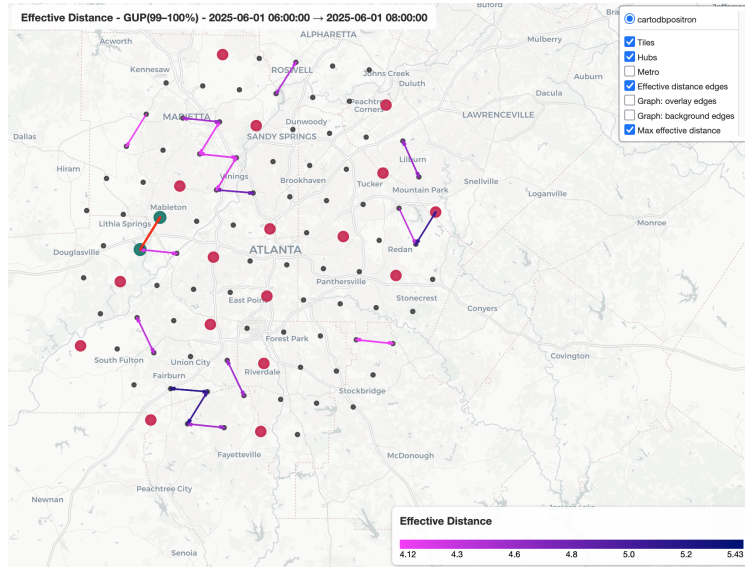


Figure 8. Synthetic effective distances for GUPs, 2025-06-01 06:00-08:00. The largest effective distance is highlighted in green.

To confirm the structural origin of this separation, Figure 9 shows the overlay network with the endpoints of the maximum effective-distance pair emphasized. Despite their spatial proximity, no direct edge connects these two locations, and they therefore constitute a GUP.

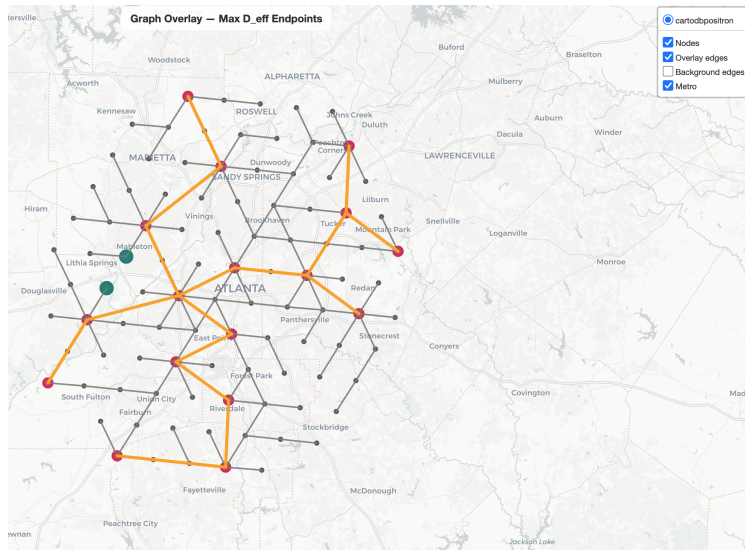


Figure 9. Overlay network highlighting the endpoints of the maximum effective-distance OD pair. The absence of a direct connection confirms that the pair is globally unconnected.

The effective-path decomposition for this OD pair is shown in Figure 10. Rather than a direct transition, flow is routed through a sequence of intermediate nodes, resulting in

a four-hop path. Two of these segments correspond to high-capacity metro edges, which dominate the probability-weighted contribution to the effective distance.



Figure 10. Effective-path decomposition for the maximum effective-distance OD pair. The dominant contribution follows a four-hop route via intermediate hubs, including two high-capacity metro-edge segments.

This example illustrates the role of effective distance as a detector of structural gaps in the network. Despite short geographic separation, the absence of a direct connection forces travel to proceed through multiple intermediates. The resulting large effective distance therefore reflects the topology and capacity structure of the network and its time-dependent dynamics, rather than spatial separation alone or aggregation artifacts.

To quantify how strongly this OD connection is supported by the underlying dynamics, we also report the total probability mass associated with all admissible return paths over the time-elapsed window. For an OD pair (i, j) , this quantity is given by

$$P_{ij}^{t_1, t_2} = \sum_{t=t_1}^{t_2} \pi_{ij}^t,$$

where π_{ij}^t is the probability that a path first reaches i from j at time-step t .

For the synthetic OD pair attaining the maximum effective distance, the total path probability over the window is

$$P_{\max}^{06:00, 08:00} = 2.09 \times 10^{-4}.$$

Thus, while the effective distance is large, the corresponding connection is realized only by a small fraction of the population, consistent with the interpretation that large effective distance reflects structurally indirect but low-probability routing through the network.

Aggregated data:

We now contrast this behavior with aggregated OD data from Mexico City. Figure 11 shows effective distances for GUP OD pairs over the time window 06:00–12:00 on 2019–09–23, corresponding to two three-hour intervals. Here and throughout, alphanumeric labels such as `9g3w6` denote geohash cell identifiers used in the NetMob dataset, and strings such as `8644c1a77fffff` denote H3 hierarchical hexagonal indices at resolution 6.

The largest effective distance observed is $D_{\max}^{\text{eff}} = 2.67$, associated with the OD pair `9g3w6` \rightarrow `9g3w0`.

In this setting, the underlying network structure is unknown and paths can only be inferred indirectly from aggregated flows. The effective-path decomposition in Fig. 12 shows that this OD pair is realized through two distinct two-step routes,

$$9g3w6 \rightarrow 9g3qx \rightarrow 9g3w0, \quad 9g3w6 \rightarrow 9g3qr \rightarrow 9g3w0.$$

The time-elapsed distance is computed as a probability-weighted average over these paths, after which the effective distance is obtained by normalization using an imputed baseline derived from geographic-distance regression.

As in the synthetic case, we compute the total probability mass associated with all admissible paths supporting this OD connection. Over the window 06:00–12:00, the aggregated-data OD pair with maximum effective distance has total path probability

$$P_{\max}^{06:00,12:00} = 1.17 \times 10^{-3}.$$

Compared to the synthetic example, this probability mass is larger, which is expected because the dominant contributing routes here are only two steps long, whereas the synthetic D_{\max}^{eff} pair is realized primarily via a four-hop route. Shorter admissible connections typically accumulate more probability mass under products of stochastic transition operators.

In addition, the coarser three-hour aggregation can further increase the effective probability of reaching the destination within the window, because each observed transition summarizes heterogeneous within-interval movements. Accordingly, elevated effective distance in the aggregated setting may reflect a superposition of multiple plausible intermediate realizations consistent with the same coarse OD flows, rather than a single sharply constrained route.

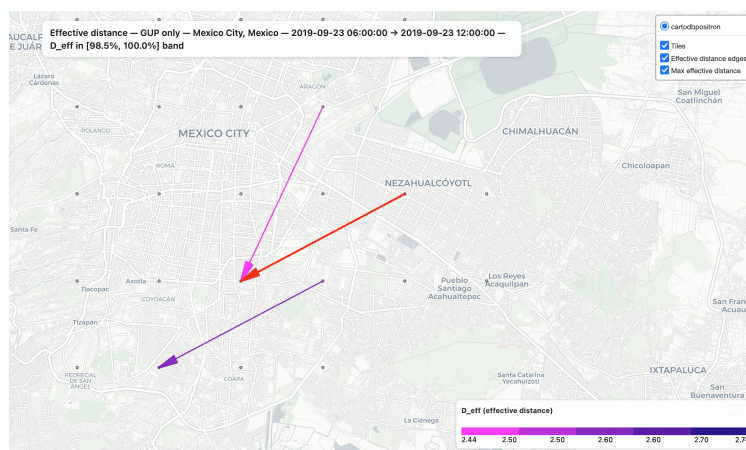


Figure 11. Mexico City: effective distances for GUPs, 2019–09–23 06:00–12:00. The maximum effective distance is $D_{\text{eff}} = 2.67$.

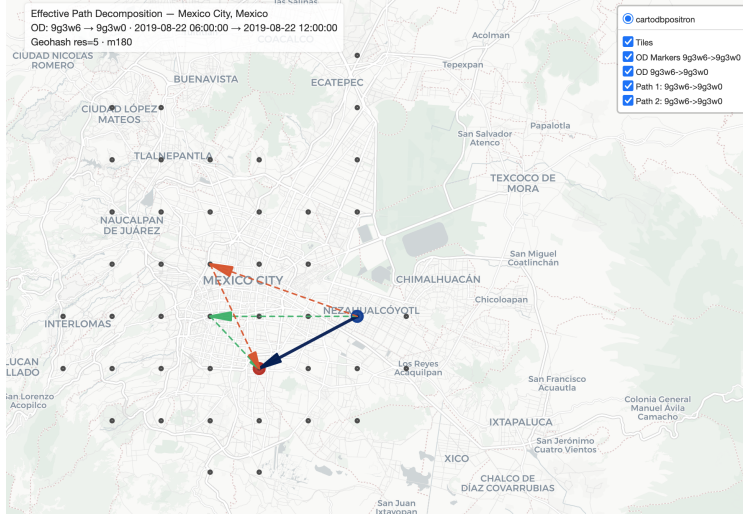


Figure 12. Aggregated-data effective-path decomposition for the OD pair $9g3w6 \rightarrow 9g3w0$. Two distinct paths contribute to the effective distance.

Comparison and role of temporal resolution:

The contrast between synthetic and aggregated results highlights the critical role of temporal resolution in effective-distance inference. In the synthetic setting, 30-minute resolution allows individual multi-hop routes to be resolved explicitly, so large effective distances can be unambiguously attributed to specific network-imposed detours. This ambiguity is a known limitation of OD-based inference under strong temporal aggregation, where multiple plausible paths may be consistent with the same observed flow [9].

In the aggregated data, transitions are observed at three-hour resolution. Within such coarse intervals, multiple distinct movement patterns may be collapsed into a single OD observation, leading to path degeneracy. As a result, elevated effective distances in the aggregated setting often arise from the superposition of several plausible intermediate paths rather than a single dominant route.

This ambiguity is therefore not a failure of the effective-distance construction. Rather, it reflects limitations imposed by coarse temporal aggregation. At higher temporal resolution, effective distance would be expected to isolate inefficient or indirect routes more sharply, in closer analogy with the synthetic case.

Overall, effective distance serves its intended purpose as a probe of *structural inefficiency* in mobility networks: it highlights OD pairs for which observed movement systematically deviates from direct or expected paths, revealing detours, bottlenecks, and constraints that are not visible from trip counts alone.

5. TIME-ELAPSED RETURN-TO-ORIGIN DISTANCE

As a complementary summary statistic to time-elapsed OD flows and effective distance, we consider the *return-to-origin* (RTO) distance. RTO measures the distance traveled by a PEP before returning to their origin within a specified time-elapsed window. When averaged across origins, RTO provides an intrinsic, population-level characterization of mobility scale, analogous in spirit to radius-of-gyration measures but derived from time-elapsed flow dynamics.

RTO is a special case of the time-elapsed OD distance construction introduced in Section 4, obtained by setting the destination equal to the origin. Throughout this section we focus on distance-based RTO; time- and speed-based variants can be obtained by the same construction with time-valued edge costs.

5.1. *Definition and variants.* RTO distance is a special case of the time-elapsed OD distance in which the destination coincides with the origin. Let $\bar{x}_{ij}^{t_1, t_2}$ denote the mean time-elapsed distance from origin j to destination i , as defined in Eq. (5) (see Appendix A). Setting $i = j$ yields the mean RTO distance for location j over the window $t_1 \leq t \leq t_2$,

$$\bar{x}_{jj}^{t_1, t_2} = \frac{\sum_{t=t_1}^{t_2} x_{jj}^t \pi_{jj}^t}{\sum_{t=t_1}^{t_2} \pi_{jj}^t}, \quad (6)$$

where x_{jj}^t and π_{jj}^t are the mean distance and probability of paths that first return to j at time-step t . The recursive computation of these quantities is summarized in Appendix A.

We distinguish two RTO variants that separate near-origin stationarity from true excursions:

- *Home RTO.* Restricts attention to paths that return to the origin at the first time-step. In this case,

$$\bar{x}_j^h = \bar{x}_{jj}^{1,2} = d_{jj}^1, \quad (7)$$

where d_{jj}^1 is the (median) distance traveled during the self-transition at location j . Home RTO therefore captures short-range, intra-cell mobility at the spatial resolution of the data.

- *Roaming RTO.* Excludes the first self-transition and conditions on paths that leave the origin before returning. The roaming RTO for location j is

$$\bar{x}_j^r = \bar{x}_{jj}^{2, t_2}, \quad (8)$$

capturing commuting- or excursion-scale mobility.

City-level RTO values are obtained by averaging over origin locations using weights induced by the aggregated OD flows at the initial time-step.

The probability that a generic PEP is located at origin j at the beginning of the window is

$$p_j^1 = \frac{\sum_i f_{ij}^1}{\sum_{i,j} f_{ij}^1}, \quad (9)$$

where f_{ij}^1 denotes the observed flow from j to i at the first time-step. As in the net-flow construction, these weights are estimated directly from observed aggregated flows at the initial time-step rather than from a fixed-point distribution. This choice ensures that RTO measures remain data-driven and applicable even when a stationary distribution is not well defined.

The relative distribution of PEPs that leave their origin at the first step is

$$p_j^r = \frac{\sum_{i \neq j} f_{ij}^1}{\sum_k \sum_{i \neq k} f_{ik}^1}, \quad (10)$$

which defines the weights used to compute the city-level *roaming RTO*:

$$\bar{x}^r = \sum_j p_j^r \bar{x}_{jj}^{2, t_2}. \quad (11)$$

Similarly, the relative distribution of PEPs that remain at their origin at the first time-step is

$$p_j^h = \frac{f_{jj}^1}{\sum_k f_{kk}^1}, \quad (12)$$

and the city-level *home RTO* is

$$\bar{x}^h = \sum_j p_j^h d_{jj}^1. \quad (13)$$

5.2. *Synthetic data.* We first examine RTO behavior in the synthetic network. As expected, home RTO is substantially smaller than roaming RTO, reflecting the distinction between near-origin stationarity and excursion-scale mobility. However, home RTO is not vanishingly small: because distances are measured at the spatial resolution of the underlying H3 grid, self-transitions correspond to movement within a cell rather than zero-length trips.

As a result, synthetic home RTO reflects typical intra-cell displacement at the chosen spatial resolution, yielding distances on the order of a single cell diameter. This behavior is consistent with the interpretation of home RTO as capturing short-range, near-origin mobility rather than literal immobility.

Figure 13 shows the synthetic *home RTO* (city average) over 2025-06-01 to 2025-06-29. The plot is shown with a zero baseline to emphasize the absolute scale of home RTO relative to roaming RTO. On this scale, day-to-day variation appears visually small.

To make these variations explicit, Figure 14 shows the same time series with a restricted vertical axis. On this scale, small but systematic fluctuations are clearly visible. In this controlled setting, variability arises from two sources: (i) intrinsic stochasticity of the time-dependent Markov dynamics, which permit randomized direction and path exploration even under a fixed transition schedule, and (ii) finite-sample effects associated with stochastic trajectory realizations in the PEP simulation.

Because transitions allow probabilistic exploration of neighboring locations, short-range return distances fluctuate over time even in the absence of structural or calendar-driven changes. These fluctuations reflect diffusion-like behavior inherent to the model rather than aggregation or measurement effects.

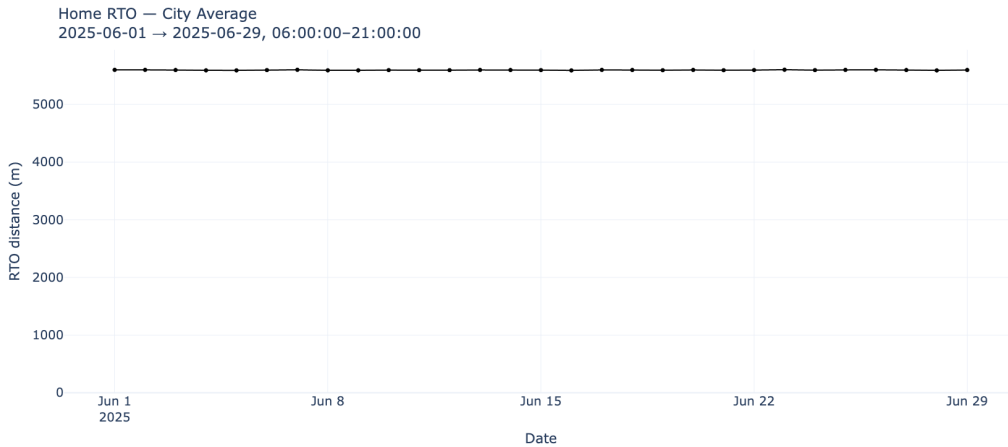


Figure 13. Synthetic home RTO, city average, 2025-06-01 to 2025-06-29. The vertical axis starts at zero to emphasize the absolute scale.

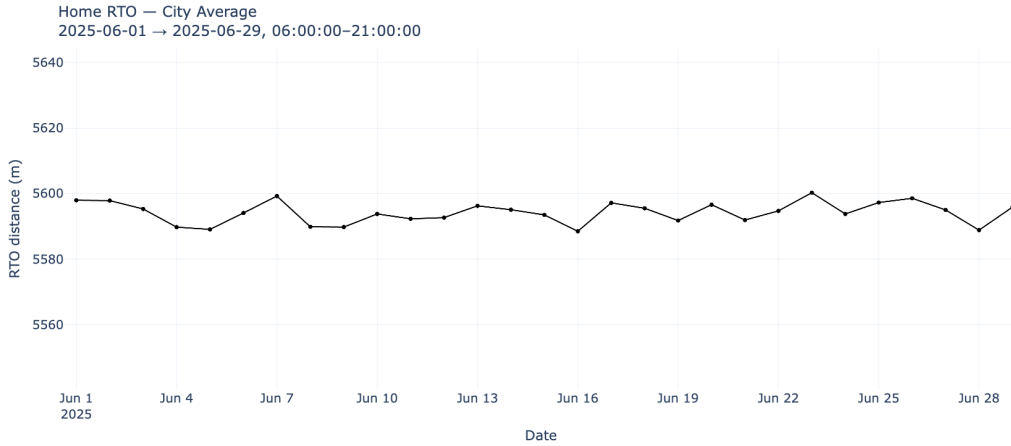


Figure 14. Synthetic home RTO, city average, shown on a restricted vertical scale. Small but persistent day-to-day fluctuations reflect intrinsic stochastic exploration of the network and finite-sample effects in trajectory realization.

Figure 15 shows the corresponding synthetic *roaming RTO* for June 2025, again plotted with a zero baseline to emphasize its absolute scale relative to home RTO. Roaming RTO is much larger than home RTO, consistent with longer excursions before return. On this scale, day-to-day variability appears modest.

Figure 16 shows the same roaming RTO time series with a restricted vertical axis. Compared to home RTO, relative fluctuations are more pronounced, reflecting the greater sensitivity of long excursion paths to stochastic routing choices, directional dispersion, and finite-sample effects in the PEP simulation. As in the home case, these variations arise under a fixed transition schedule and do not reflect structural or calendar-driven changes.

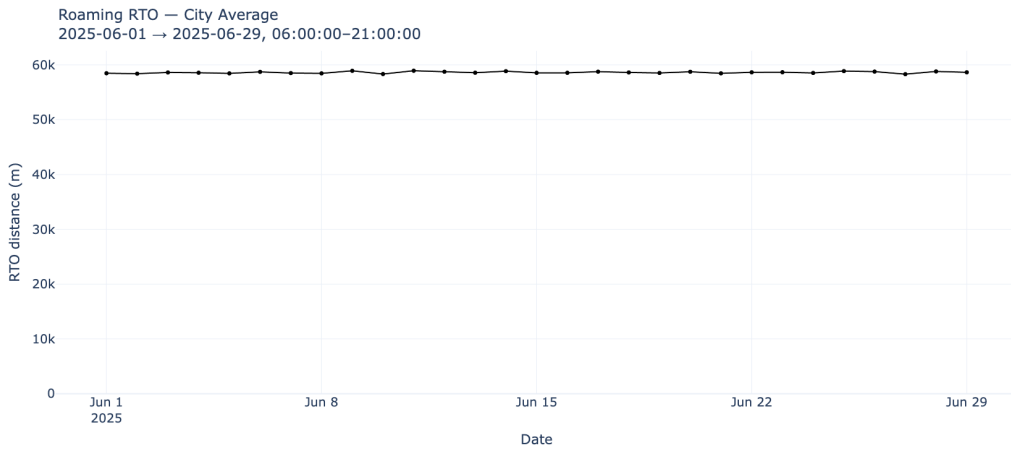


Figure 15. Synthetic roaming RTO, city average, 2025-06-01 to 2025-06-29.



Figure 16. Synthetic roaming RTO, city average, shown on a restricted vertical scale. Relative fluctuations are larger than for home RTO, reflecting stochastic path exploration over longer excursion distances under fixed Markov dynamics.

This mechanism mirrors the limited stochastic variability observed in synthetic effective-distance time sweeps, reinforcing the interpretation that both measures reflect stable underlying dynamics perturbed by probabilistic path exploration.

5.3. *Aggregated data: Mexico City.* We now compute RTO from aggregated OD data for Mexico City over 2019 using the time-elapsd window 06:00–21:00. As in the synthetic case, home RTO is much smaller than roaming RTO, reflecting the distinction between near-origin stationarity and excursion-scale mobility.

Figure 17 shows the *home RTO* (city average). Home RTO varies over time, but the weekday–weekend modulation is comparatively muted, consistent with the interpretation that near-origin movement is less sensitive to commuting schedules than longer excursions. This contrast mirrors the effective-distance diagnostics: measures dominated by local or near-origin movement are less sensitive to calendar-driven mobility patterns than those capturing longer excursions.

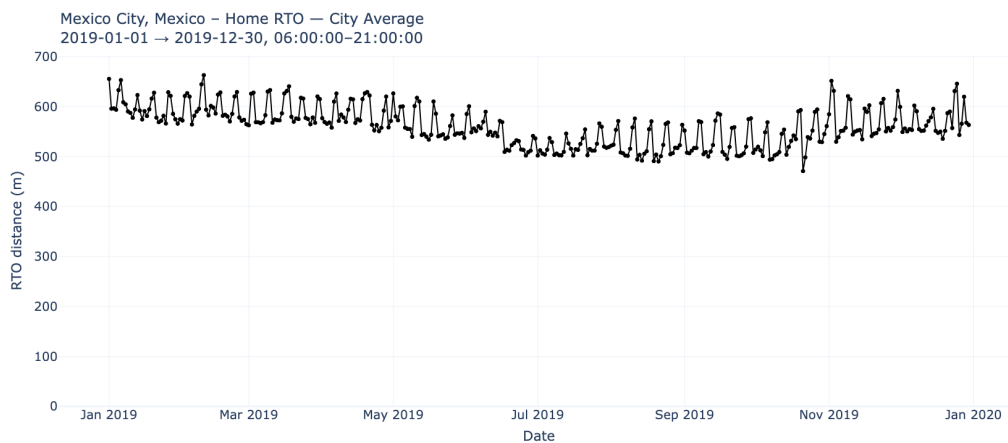


Figure 17. Mexico City home RTO, city average, 2019.

Figure 18 shows the corresponding *roaming RTO*. Here the weekday–weekend signature is much more pronounced, consistent with roaming RTO capturing commute-like excursions and longer out-and-back trips. In addition, both home and roaming RTO exhibit slower variations across the year. These may reflect seasonal effects, changing activity patterns, or other contextual factors (e.g., holidays and events). We do not attempt to attribute these variations causally in this work.

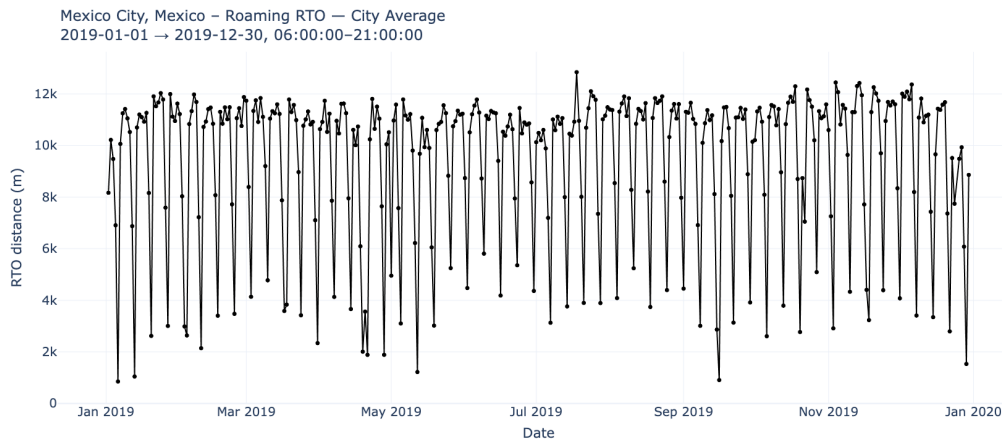


Figure 18. Mexico City roaming RTO, city average, 2019.

Finally, the aggregated setting introduces measurement effects absent in the synthetic model. With three-hour time steps, multiple within-interval movements are compressed. Distance statistics must therefore be derived from reported trip-distance summaries (e.g., medians) rather than controlled edge-length means. These factors can amplify apparent variability and blur fine-scale temporal structure, particularly for roaming RTO, which is driven by longer excursions.

A detailed empirical analysis of RTO behavior across cities, temporal regimes, and aggregation scales is left for future work. The definitions provided here demonstrate that such measures are naturally supported by the time-elapsed framework and can be computed without access to individual trajectories.

6. CONCLUSION

This paper addresses the problem of extracting longer-term mobility structure from space- and time-aggregated collective OD data. Starting from a pseudo Markov-chain representation of aggregated flows, we develop a consistent framework for constructing time-elapsed mobility measures, including net OD flows, time-elapsed distance, effective distance, and RTO quantities, without relying on individual trajectories or path-level observations.

Despite the well-known mobility-aliasing effects induced by coarse temporal aggregation in datasets such as NetMob 2024, we show that meaningful structure can still be recovered. Time-elapsed net OD flows reproduce expected large-scale commuting patterns, providing a qualitative consistency check for the framework. These flows are not imposed a priori but emerge from the repeated application of time-dependent transition operators inferred from aggregated data.

Time-elapsed effective distance offers a complementary perspective by highlighting OD pairs whose realized travel is systematically more indirect than expected given their geographic separation. Through comparisons between synthetic data and aggregated real-world data, we show that effective distance successfully identifies structurally indirect connections, including GUPs. In the synthetic setting, where network structure and temporal resolution are fully controlled, effective distances are stable and directly attributable to known routing constraints. In aggregated data, effective distances reflect a superposition of plausible paths within coarse time windows, leading to greater variability and ambiguity. These differences underscore the central role of temporal resolution in interpreting higher-order mobility measures. This observation is consistent with prior work emphasizing the inherently multiscale nature of human mobility and the dependence of inferred structure on the chosen spatial and temporal scales [33].

While effective distance can exhibit apparent spatial and temporal recurrence in both settings, we emphasize that this work does not perform a formal persistence or flow analysis. Observed recurrence should therefore be interpreted as a diagnostic signal rather than a definitive indicator of structural persistence. Formal persistence and flow-based characterizations require additional assumptions and dedicated analytical frameworks, which lie outside the scope of the present work (e.g., [35]). Nevertheless, effective distance appears to serve its intended role as a probe for indirect, inefficient, or constrained mobility, pointing to OD pairs where detours, transfers, or network limitations may be at play.

RTO distance measures extend the framework to capture the typical spatial scale of excursions encoded in aggregated dynamics. Home and roaming RTO distances separate near-origin activity from longer-range movement and provide a collective analogue of individual radius-of-gyration concepts. In aggregated data, RTO measures are influenced by temporal resolution, summary statistics of trip length, and contextual effects such as weekday–weekend structure and seasonal variation. Accordingly, RTO is best viewed here as a first-order descriptive quantity, with more detailed interpretation deferred to settings with higher-resolution or complementary data.

At sufficiently large spatial and temporal scales, the existence of stationary or slowly evolving distributions in the pseudo Markov-chain model suggests the possibility, in principle, of identifying long-term drift or relocation of populations, should data with appropriate resolution and coverage become available. Such collective signals would not correspond to individual migration decisions, but rather to system-level reorganization emerging from repeated, structured flows over time. This perspective resonates, at a qualitative level, with anthropological accounts in which seasonal mobility, redistribution, and long-horizon movement play a role in shaping social organization and settlement patterns (e.g., [26]).

In the context of the NetMob 2024 dataset, a natural application is the identification of large-scale population drift and structurally constrained movement patterns. With additional data sources, such analyses could inform questions relevant to several Sustainable Development Goals [27], including SDG 8 (Decent Work and Economic Growth), SDG 9 (Industry, Innovation and Infrastructure), SDG 11 (Sustainable Cities and Communities), and SDG 13 (Climate Action). Future work may also explore extensions beyond the pseudo-Markov assumption, incorporating additional constraints or temporal dependencies to better reflect real-world mobility dynamics. Time-elapsed mobility measures of the type developed here may serve as complementary inputs to applied studies of urban dynamics, accessibility,

and infrastructure efficiency, where aggregated data are increasingly used to inform planning and policy [28–30].

CODE AVAILABILITY

All code used to compute the time-elapsd mobility measures reported in this paper is available as open-source software at github.com/asif-shakeel/Network-Mobility-Measures.

ACKNOWLEDGMENTS

The authors would like to acknowledge productive participation from the members of David Meyer’s research group, in particular, Itai Maimon for initiating the discussion that led to the RTO definition, Orest Bucicovschi, David Rideout and Jiajie Shi.

Mobility data were provided by Cuebiq and made available through the NetMob 2024 Data Challenge. All data were anonymized and aggregated prior to release. Cuebiq does not review, endorse, or take responsibility for the analyses or conclusions presented in this work.

REFERENCES

- [1] Y. de Montjoye, S. Gamsbs, V. Blondel, G. Canright, N. de Cordes, S. Deletaille, K. Engø-Monsen, M. Garcia-Herranz, J. Kendall, C. Kerry, G. Krings, E. Letouzé, M. Luengo-Oroz, N. Oliver, L. Rocher, A. Rutherford, Z. Smoreda, J. Steele, E. Wetter, A. Pentland, and L. Bengtsson, *On the privacy-conscious use of mobile phone data*, Scientific Data **5** (2018), no. 1. doi:10.1038/sdata.2018.286.
- [2] F. Xu, Z. Tu, Y. Li, P. Zhang, X. Fu, and D. Jin, *Trajectory Recovery From Ash: User Privacy Is NOT Preserved in Aggregated Mobility Data*, Proceedings of the 26th International Conference on World Wide Web, 2017, pp. 1241–1250. doi:10.1145/3038912.3052620.
- [3] C. Buckee, S. Balsari, J. Chan, M. Crossas, F. Dominici, U. Gasser, Y. Grad, B. Grenfell, M. Halloran, M. Kraemer, M. Lipsitch, C. Metcalf, L. Meyers, T. Perkins, M. Santillana, S. Scarpino, C. Viboud, A. Wesolowski, and A. Schroeder, *Aggregated mobility data could help fight COVID-19*, Science **368** (2020), no. 6487, 145-146. doi:10.1126/science.abb8021.
- [4] M. Tizzoni, P. Bajardi, C. Poletto, J. J. Ramasco, D. Balcan, B. Gonçalves, N. Perra, and V. Colizza, *Real-time numerical forecast of global epidemic spreading: Case study of 2009 A/H1N1pdm*, BMC Medicine **10** (2012), 165. doi:10.1186/1741-7015-10-165.
- [5] D. Kondor, B. Hashemian, Y. de Montjoye, and C. Ratti, *Towards Matching User Mobility Traces in Large-Scale Datasets*, IEEE Transactions on Big Data **6** (2020), no. 4, 714-726. doi:10.1109/TBDDATA.2018.2871693.
- [6] M. Barthélemy, *Spatial networks*, Physics Reports **499** (2011), no. 1–3, 1–101. doi:10.1016/j.physrep.2010.11.002.
- [7] M. Batty, *The New Science of Cities*, MIT Press, Cambridge, MA, 2013. ISBN 978-0262019521.
- [8] M. González, C. Hidalgo, and A. Barabási, *Understanding individual human mobility patterns*, Nature **453** (2008), 779-782. doi:10.1038/nature06958.
- [9] H. Barbosa, M. Barthelemy, G. Ghoshal, C. James, M. Lenormand, T. Louail, R. Menezes, J. Ramasco, F. Simini, and M. Tomasini, *Human mobility: Models and applications*, Physics Reports **734** (2018), 1-74. doi:10.1016/j.physrep.2018.01.001.
- [10] D. Brockmann, L. Hufnagel, and T. Geisel, *The scaling laws of human travel*, Nature **439** (2006), no. 7075, 462-465. doi:10.1038/nature04292.
- [11] B. Jiang, J. Yin, and S. Zhao, *Characterizing the human mobility pattern in a large street network*, Phys. Rev. E **80** (2009), 021136. doi:10.1103/PhysRevE.80.021136.
- [12] N. Williams, T. Thomas, M. Dunbar, N. Eagle, and A. Dobra, *Measures of Human Mobility Using Mobile Phone Records Enhanced with GIS Data*, PLOS ONE **10** (2015), no. 7, 1-16. doi:10.1371/journal.pone.0133630.
- [13] *NetMob 2024*. url:netmob.org.

- [14] T. Yabe, M. Luca, K. Tsubouchi, B. Lepri, M. Gonzalez, and E. Moro, *Enhancing human mobility research with open and standardized datasets*, *Nat Comput Sci* **4** (2024), 469-472. doi:10.1038/s43588-024-00650-3.
- [15] C. Balzotti, A. Bragagnini, M. Briani, and E. Cristiani, *Understanding Human Mobility Flows from Aggregated Mobile Phone Data*, *IFAC-PapersOnLine* **51** (2018), no. 9, 25-30. doi:10.1016/j.ifacol.2018.07.005.
- [16] C. Peng, X. Jin, K. Wong, M. Shi, and P. Liò, *Collective Human Mobility Pattern from Taxi Trips in Urban Area*, *PLOS ONE* **7** (2012), no. 4, 1-8. doi:10.1371/journal.pone.0034487.
- [17] B. Guo, H. Yang, H. Zhou, Z. Huang, F. Zhang, L. Xiao, and P. Wang, *Understanding individual and collective human mobility patterns in twelve crowding events occurred in Shenzhen*, *Sustainable Cities and Society* **81** (2022), 103856. doi:10.1016/j.scs.2022.103856.
- [18] M. Flores-Garrido, G. de Anda-Jáuregui, P. Guzmán, A. Meneses-Viveros, A. Hernández-Álvarez, E. Cruz-Bonilla, and M. Hernández-Rosales, *Mobility networks in Greater Mexico City*, *Scientific Data* **11** (2024), 84. doi:10.1038/s41597-023-02880-y.
- [19] S. Milusheva, E. zu Erbach-Schoenberg, L. Bengtsson, E. Wetter, and A. Tatem, *Understanding the Relationship between Short and Long Term Mobility*, *AFD Research Paper Series* **2017-69** (2017).
- [20] David A. Meyer and Asif Shakeel, *Mobility Trajectories from Network-Driven Markov Dynamics*, arXiv preprint (2026), available at [arXiv:2601.06020](https://arxiv.org/abs/2601.06020).
- [21] J. Norris, *Markov Chains*, Cambridge Series in Statistical and Probabilistic Mathematics, Cambridge University Press, New York, 1997. doi:10.1017/CBO9780511810633.
- [22] N. Masuda and P. Holme, *Temporal Network Epidemiology*, Springer (2017). ISBN 978-981-10-5286-8.
- [23] W. Zhang, M. Nunez del Prado, V. Gauthier, and S. Milusheva, *The NetMob2024 Dataset: Population Density and OD Matrices from Four LMIC Countries* (2024). doi:10.48550/arXiv.2410.00453.
- [24] Uber Technologies, Inc., *H3: A Hexagonal Hierarchical Geospatial Indexing System*, 2018. <https://h3geo.org/>.
- [25] D. Brockmann and D. Helbing, *The hidden geometry of complex, network-driven contagion phenomena*, *Science* **342** (2013), no. 6164, 1337-1342. doi:10.1126/science.1245200.
- [26] D. Graeber and D. Wengrow, *The dawn of everything: a new history of humanity*, Farrar, Straus and Giroux, New York, 2021. WorldCat:1255689164.
- [27] *Sustainable Development Goals*. url:undp.org/sustainable-development-goals.
- [28] C. Yang, H. Sutrisno, A. Chan, H. Tampubolon, and B. Wibowo, *Identification and Analysis of Weather-Sensitive Roads Based on Smartphone Sensor Data: A Case Study in Jakarta*, *Sensors* **21** (2021), no. 7. url:www.mdpi.com/1424-8220/21/7/2405.
- [29] Y. Yang, A. Pentland, and E. Moro, *Identifying latent activity behaviors and lifestyles using mobility data to describe urban dynamics*, *EPJ Data Science* **12** (2023), no. 1, 2193-1127. doi:10.1140/epjds/s13688-023-00390-w.
- [30] T. Wang, Y. Li, I. Chuang, W. Qiao, J. Jiang, and L. Beattie, *Evaluating the 15-minute city paradigm across urban districts: A mobility-based approach in Hamilton, New Zealand*, *Cities* **151** (2024), 105147. doi:10.1016/j.cities.2024.105147.
- [31] N. Higham and L. Lin, *On pth roots of stochastic matrices*, *Linear Algebra and its Applications* **435** (2011), no. 3, 448-463. doi:10.1016/j.laa.2010.04.007.
- [32] E. Deza and M. Deza, *Encyclopedia of Distances*, Springer-Verlag, Berlin, 2009. doi:10.1007/978-3-642-00234-2.
- [33] L. Alessandretti, U. Aslak, and S. Lehmann, *The scales of human mobility*, *Nature* **587** (2020), no. 7834, 402-407. doi:10.1038/s41586-020-2909-1.
- [34] U. Fugacci, S. Scaramuccia, F. Iuricich, and L. Floriani, *Persistent Homology: a Step-by-step Introduction for Newcomers*, Smart Tools and Apps for Graphics - Eurographics Italian Chapter Conference, 2016. doi:10.2312/stag.20161358.
- [35] X. Chen and J. Lai, *Detecting abnormal crowd behaviors based on the div-curl characteristics of flow fields*, *Pattern Recognition* **88** (2019), 342-355. doi:10.1016/j.patcog.2018.11.023.

APPENDIX A. RECURSIVE COMPUTATION OF TIME-ELAPSED OD DISTANCES

This appendix provides the technical details underlying the computation of time-elapsed OD distances used in Section 4.1. The purpose of this appendix is to make explicit how path probabilities and path lengths are propagated through time while excluding trivial loops through the origin and destination.

A.1. *Path probabilities.* Fix an ordered OD pair (j, i) . We track admissible paths that originate at j at time $t = 0$ and terminate at i at some later time-step, without passing through either i or j at any intermediate time-step. In the following, the superscripts i, j simply keep track of the OD pair under consideration and can be regarded as bookkeeping.

Let $M^t = [m_{kr}^t]$ denote the time-dependent stochastic transition matrix at time-step t , defined in Eq. (2). We define the vector

$$\mathbf{p}^{i,j,t} = [p_k^{i,j,t}],$$

where $p_k^{i,j,t}$ is the probability that a path starting at j reaches node k at time-step t without having previously visited either i or j .

Initialization is given by

$$\mathbf{p}^{i,j,1} = [m_{kj}^1],$$

that is, the j -th column of M^1 .

For $t \geq 2$, probabilities propagate according to

$$p_k^{i,j,t} = \sum_{r:r \neq i,j} m_{kr}^t p_r^{i,j,t-1}.$$

To write this as a matrix operation, define the masked vector

$$\tilde{\mathbf{p}}^{i,j,t} = [\tilde{p}_k^{i,j,t}],$$

where

$$\tilde{p}_k^{i,j,t} = \begin{cases} p_k^{i,j,t}, & \text{if } k \neq i, j, \\ 0, & \text{otherwise.} \end{cases}$$

Then

$$\mathbf{p}^{i,j,t} = M^t \tilde{\mathbf{p}}^{i,j,t-1}.$$

Simplifying notation, let

$$\pi_{ij}^t = p_i^{i,j,t}$$

denote the probability that a path starting at j first reaches i at time-step t , without intermediate returns to j .

A.2. *Path distances.* Let d_{kr}^t denote the distance traveled between locations r and k at time-step t , as reported by the OD data. For the same admissible paths used above, we keep track of mean path lengths to each node k . Define

$$\mathbf{y}^{i,j,t} = [y_k^{i,j,t}],$$

where $y_k^{i,j,t}$ is the mean distance traveled by admissible paths from j to k that arrive at time-step t , and take $y_k^{i,j,0} = 0$.

For $t \geq 1$, distances propagate via the probability-weighted update

$$y_k^{i,j,t} = \frac{1}{p_k^{i,j,t}} \sum_{r:r \neq i,j} (d_{kr}^t + y_r^{i,j,t-1}) m_{kr}^t p_r^{i,j,t-1}, \quad (14)$$

whenever $p_k^{i,j,t} > 0$.

We can also organize this computation as matrix operations. Define a matrix

$$\tilde{D}^{i,j,t} = [\tilde{d}_{kr}^{i,j,t}],$$

where

$$\tilde{d}_{kr}^{i,j,t} = \frac{d_{kr}^t + y_r^{i,j,t-1}}{p_k^{i,j,t}},$$

whenever $p_k^{i,j,t} > 0$. Then the distance update can be written as

$$\mathbf{y}^{i,j,t} = [\tilde{D}^{i,j,t} \cdot M^t] \tilde{\mathbf{p}}^{i,j,t-1},$$

where \cdot denotes element-by-element multiplication, followed by the usual matrix product.

Again simplifying notation, let

$$x_{ij}^t = y_i^{i,j,t}$$

denote the mean distance traveled by paths that start at j and first reach i at time-step t , without intermediate returns to j .

A.3. Time-elapsd averaging. The mean time-elapsd distance traveled from j to i over a window $t_1 \leq t \leq t_2$ is defined by

$$\bar{x}_{ij}^{t_1,t_2} = \frac{\sum_{t=t_1}^{t_2} x_{ij}^t \pi_{ij}^t}{\sum_{t=t_1}^{t_2} \pi_{ij}^t}, \quad (15)$$

which matches Eq. (5) in the main text.

Replacing step distances d_{kr}^t by step travel times yields the analogous time-elapsd travel-time quantity.

A.4. Remarks.

- The exclusion of intermediate visits to i and j prevents trivial self-loops from biasing the estimate.
- The construction applies equally to travel time by replacing d_{kr}^t with single-step travel times.

APPENDIX B. CONCEPTUAL APPROACHES TO MITIGATING MOBILITY ALIASING

This appendix outlines a conceptual direction for mitigating mobility-aliasing rather than a method used in the present analysis. The time-resolution of data could be improved by changing the intervals of data aggregation to be shorter, commensurate with a statistically useful measure of speed, perhaps a standard deviation above the mean speed. Suppose that speed is known and translates to an interval time of T minutes. The aggregation would record the trips that start in an interval mT to $(m+1)T$ and end in an interval nT to $(n+1)T$. For each m and origin there will only be finitely many n and destinations. The record would thus be indexed by the OD pair and m and n (equivalently mT and nT), a quadruple of indices, and include as data quantities of interest like trip-count, the mean (or median) time and distance traveled. The mean/median for the traveled time would likely be longer than the interval and those for distance could be shorter or longer than the spatial resolution of the geohash. This approach, while not eliminating mobility-aliasing, would help reduce it.

In the present case, the time-resolution, as noted, is coarser than needed, and potentially leads to aliasing in user and trip counts. To account for the aliasing, we could try the

following idea. Continuing with the example of 3-hour, GH5, we assume that the dynamics of movements are slowly changing, at 3-hour intervals. For each coarse time-step, we need to insert p transition matrices, one for each finer interval, such that their product is the original transition matrix. Denote by H_k the finer-resolution transition matrices where $k = 1, \dots, p$. Omitting the superscript t for the original time-step, and writing $M = M^t$,

$$M = \prod_{k=1}^p H_k.$$

A more stringent version of this is if all the finer resolution matrices are assumed to be the same, i.e., $H_k = H$. Then

$$M = H^p.$$

Such a stochastic matrix H is called the p -th root of a stochastic matrix M . It might not exist, however, and finding one is a challenge [31].

An approximation might be attempted in finding the p -th root, in some distance or distance-like measure. Let the measure be K . The optimal approximation to the root would correspond to the minimum distance achievable over the space of stochastic matrices. Let the minimum distance be K_{\min} :

$$K_{\min} = \min_{B: B \text{ stochastic}} K(M, B^p).$$

Then the optimal approximation is \hat{H} such that:

$$K(M, \hat{H}^p) = K_{\min}.$$

Among such measures could conceivably be the Relative Entropy (Kullback-Leibler divergence) or the Frobenius distance [32]. The authors have not been able to find fast converging algorithms for the approximation for the size of stochastic matrices in this paper.

In summary, we would need to iterate p times the approximate stochastic p -th root of the 3-hourly transition matrix, where p is the number of shorter steps in the 3-hour interval. For instance, $p = 4$ if the shorter interval is 45 minutes. The reason for choosing the approximate p -th root is so that the transition probabilities at the 3-hour interval are consistent with it. We expect it to yield different estimates for the distance and time measures that we have developed than those using the 3-hourly transition matrix, for the reason that mean trip-distance and trip-times are additive over path segments. Developing and analyzing such approximation schemes rigorously is a natural direction for future work.

APPENDIX C. SUPPLEMENTARY DIAGNOSTICS FOR EFFECTIVE DISTANCE

C.1. Time sweep of high effective-distance OD pairs. We examine temporal recurrence of high effective-distance events using time sweeps of GUPs. These visualizations are intended as diagnostics rather than inferential results.

Synthetic data:

Figure 19 shows a time sweep of effective distances for synthetic GUPs over the period 2025-06-01 to 2025-06-29, for the time-elapsing window 06:00-08:00 (four 30-minute steps). OD pairs shown fall within the top 99th percentile of effective distance on each day. To suppress contributions from extremely unlikely paths that arise purely from stochastic noise,

we apply a probability cutoff before computing percentile bands. Specifically, OD pairs are retained only if the total path-hit probability satisfies

$$P_{ij}^{t_1, t_2} = \sum_{t=t_1}^{t_2} \pi_{ij}^t \geq 10^{-6}.$$

This threshold is chosen arbitrarily and is meant to remove numerically negligible connections while preserving all structurally meaningful high effective-distance events.

The synthetic dynamics exhibit a largely regular temporal structure, but with non-negligible variability in effective-distance magnitudes across days. The same set of OD pairs appears persistently throughout the period, and recurrence frequencies are highly uniform across pairs. However, effective distances for a given OD pair are no longer perfectly constant in time.

This variability arises from intrinsic stochastic exploration of the network under the Markov dynamics, compounded by finite-sample effects in realized trajectory ensembles within each time bin. Although the underlying transition kernels are strictly periodic and admit a periodic fixed point at the population level, effective distances are computed from realized path ensembles. Distance sampling within resolution-dependent envelopes introduces controlled fluctuations in path lengths, while preserving the overall ranking and temporal persistence of high effective-distance OD pairs.

As a result, the synthetic time sweep reflects a periodic dynamical regime with structured stochastic variability: recurrence is highly regular, while effective-distance magnitudes exhibit bounded fluctuations driven by trajectory-level randomness rather than changes in the transition dynamics.

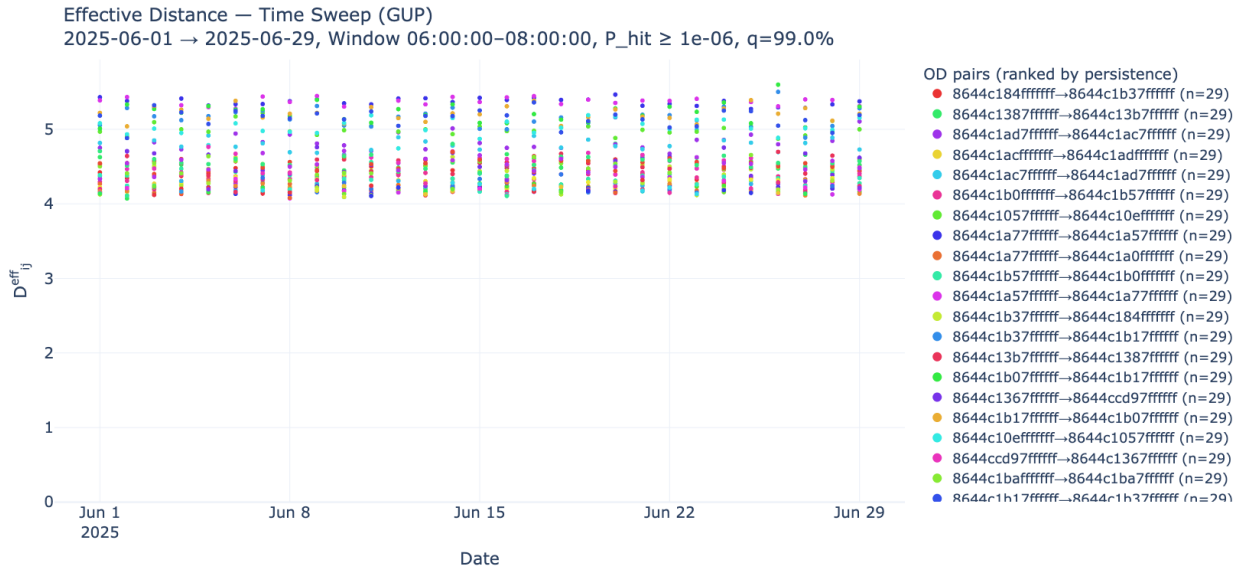


Figure 19. Synthetic time sweep of effective distances for GUPs. OD pairs recur with nearly uniform frequency across days, while effective distance magnitudes exhibit bounded variability due to stochastic path realizations within a periodic transition structure.

Aggregated data:

Figure 20 shows the corresponding time sweep for Mexico City aggregated OD data over 2019, for the time-elapsd interval 06:00–09:00–12:00. As in the synthetic case, OD pairs shown fall within the top 99th percentile on each day. Again, we apply a probability cutoff before computing percentile bands. Only those OD pairs are retained whose total path-hit probability satisfies

$$P_{ij}^{t_1,t_2} = \sum_{t=t_1}^{t_2} \pi_{ij}^t \geq 10^{-6}.$$

This cutoff is identical to that used in the synthetic case and serves the same diagnostic purpose.

In contrast to the synthetic setting, recurrence and effective-distance magnitudes are both highly heterogeneous. Some OD pairs appear frequently, while others occur sporadically, and effective distances for a given OD pair vary substantially across days.

Several factors contribute to this irregularity. First, the aggregated data are observed at a coarse temporal resolution (three-hour intervals), within which multiple distinct movement patterns may be collapsed into a single OD observation. Second, baseline distances are estimated using median trip lengths rather than means, reflecting reporting constraints in the data. Third, multi-path ambiguity is unavoidable: multiple plausible intermediate routes may contribute to a single effective-distance estimate.

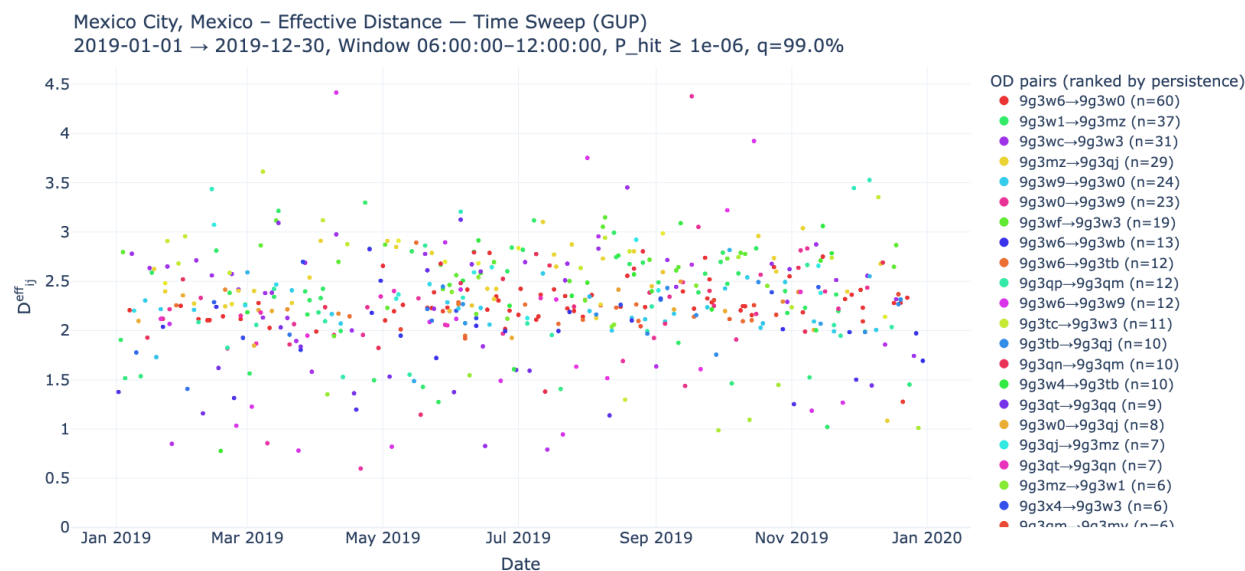


Figure 20. Mexico City time sweep of effective distances for GUPs. Both recurrence frequencies and effective-distance magnitudes vary substantially across OD pairs and across days, reflecting temporal aggregation and path ambiguity.

Interpretation:

The contrast between the two settings highlights the role of temporal aggregation and stochastic structure in shaping effective-distance dynamics. In the synthetic model, variability in effective distances arises solely from trajectory-level sampling within a fixed, periodic transition process. This produces bounded fluctuations around stable, recurrent OD pairs.

In the aggregated data, by contrast, variability reflects a superposition of heterogeneous behaviors, including weekday–weekend effects, irregular events, seasonal patterns, and context-dependent travel, all observed at relatively coarse temporal resolution. As a result, neither the recurrence of high effective-distance OD pairs nor their effective-distance magnitudes remain stable over time.

While we do not perform a formal persistence or multiscale analysis, the repeated appearance of certain OD pairs with high effective distance across days and overlapping time windows suggests that such measures may exhibit structure across temporal scales, a topic of interest in human mobility research [33]. This observation motivates future work using persistence-based approaches to characterize such structures more systematically [34, 35].